Optimising laser absorption tomography beam arrays for imaging chemical species in gas turbine engine exhaust plumes

D. McCormick[a], M.G. Twynstra[b], K.J. Daun[b], H. McCann[c]

[a]*School of Electrical and Electronic Engineering, University of Manchester, United Kingdom*
[b]*Department of Mechanical and Mechatronics Engineering, University of Waterloo, Canada*
[c]*School of Engineering, University of Edinburgh, United Kingdom*

Abstract

This paper will describe the application of resolution matrices to the design of an optimised 126 beam, 6m absorption tomography array for imaging concentrations of CO_2 in the exhaust plume of a Rolls-Royce Trent 1000 gas turbine engine. The resolution matrix will be used to define a fitness value, which is a function of the beam configuration, and is minimised by the optimal beam arrangement. Constraints ensure that the optimised beam arrangement can be implemented in a real tomography system. Genetic algorithms are used to determine the optimal array design from the large problem set.
Results for image reconstructions of a quasi-realistic phantom of the exhaust plume for each of the array designs are presented with indications of the reconstruction errors. From the results, conclusions are drawn on the suitability of applying resolution matrices to the design of beam arrays for real limited-data tomographic systems.

Keywords: absorption tomography, array design, image reconstruction, chemical species, gas turbine engines

1. Introduction

The optimum layout of sparse beam arrays is a long-recognised problem in limited-data hard-field tomography. In the case of laser absorption tomography, reconstruction accuracy depends strongly on the arrangement of laser beams transecting the flow field [1-3]. This is a particular problem for large industrial tomography processes, for example those associated with imaging in gas turbine exhaust plumes, where geometric considerations exacerbate the limited-data nature of the problem.

Existing optimisation methods for beam array design have centred on using the heuristic approach of distributing the beam layout in the sinogram space to increase the angular range of the beams in the imaging space and hence improve the image reconstruction and imaging performance of a tomographic system [4]. Whilst this heuristic approach has been demonstrated to work well for small physical geometries and low beam counts, it becomes more complicated to apply for arrays spanning several metres and including in excess of 100 beams resulting in beam array designs that cannot be determined as optimal.

Recent work on beam arrangement optimisation for absorption tomography has sought to provide a structured mathematical approach to array design by understanding the underlying mathematical properties of the linear problem using resolution matrices [5]. Simulated results of beam array optimisations using resolution matrices has been demonstrated to give improved beam array layout over heuristic methods, however to date it has not been applied to the design of a real laser absorption tomography beam array.

The FLITES (Fibre-Laser Imaging of Turbine Exhaust Species) project [6] is an industry-academia consortium concerned with in-plume imaging of chemical species of interest to the aviation community, specifically CO_2 and Unburnt Hydrocarbons (UHCs), using laser absorption tomography. The FLITES project will realise the development of a large-scale (imaging space of several metres) and large beam number (100+ beams) system for imaging concentrations of CO_2 in the exhaust plume of a Rolls-Royce Trent 1000 gas turbine engine.

This paper will describe a structured approach to the design of an optimised 126 beam, 6m absorption tomography array for the FLITES project using resolution matrices and real physical design constraints. Reconstructed images for a quasi-realistic phantom will be presented which will permit a determination of the suitability of this approach to the design of optimal beam arrays for real limited-data tomographic systems.

Nomenclature

$b(\Phi)$	attenuation of i^{th} beam
$I_{\eta 0,i}$	incident intensity of i^{th} beam
$I_{\eta,i}$	exiting intensity of i^{th} beam
κ_n	absorption coefficient
$\mathbf{r}_{\Phi i}(u)$	position vector of i^{th} beam
$\mathbf{A}$	sensitivity matrix
$\mathbf{A}^{\#}$	regularised inverse of $\mathbf{A}$
λ	relaxation parameter
$\mathbf{L}$	regularisation matrix
$\mathbf{x}^{\mathbf{exact}}$	exact solution
$\mathbf{x}_{\lambda}$	reconstructed solution
$\boldsymbol{\delta}\mathbf{b}$	noise
$\mathbf{R}$	resolution matrix of beam array
F	fitness value of beam array

2. Absorption tomography for gas turbine engines

The theory of absorption tomography has been outlined in the literature [7]. Near-IR Absorption Tomography (NIRAT) systems have been described demonstrating the application of laser absorption tomography for imaging a range of chemical species in hostile environments [2,8-9].

2.1. Principles of absorption tomography

Absorption tomography is an optical tomography technique which exploits the absorption characteristic of certain molecules using lasers at spectroscopically targeted wavelengths [10]. The arrangement for a single laser beam, from launch to receive optics, transecting a tomography imaging space is illustrated in Fig. 1:

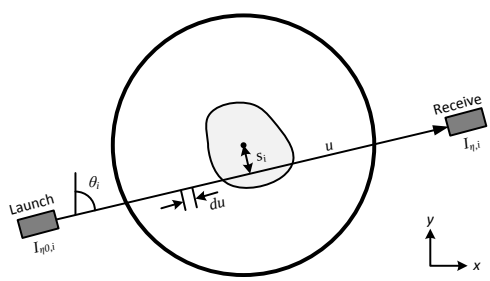

Fig. 1. Representation of i^{th} beam from a launch to receive across tomography imaging space.

For the interaction of the laser beam with an absorbing feature, the beam attenuation as a function of the incident and exiting beam intensity at the launch and receive respectively is given by the Beer-Lambert law:

$$b(\Phi_i) = \ln\left(\frac{I_{\eta_0,i}}{I_{\eta,i}}\right) = \int_0^{\infty} \kappa_{\eta}\left[\mathbf{r}_{\Phi_i}(u)\right] du \tag{1}$$

The position of the beams can be expressed in sinogram space as a function of the position relative to the imaging space origin, S_i, and the beam angle with respect to the y-axis, θ_i. The spread of these beams in the sinogram space is critical to sampling the imaging space in order to improve the reconstruction quality [4,11].

2.2. Geometric arrangement for in-plume imaging using absorption tomography

The FLITES beam array is targeted at imaging CO_2 concentrations in the exhaust plume of a Rolls-Royce Trent 1000 gas turbine engine. The geometric arrangement of the beam array and engine is illustrated in Fig. 2:

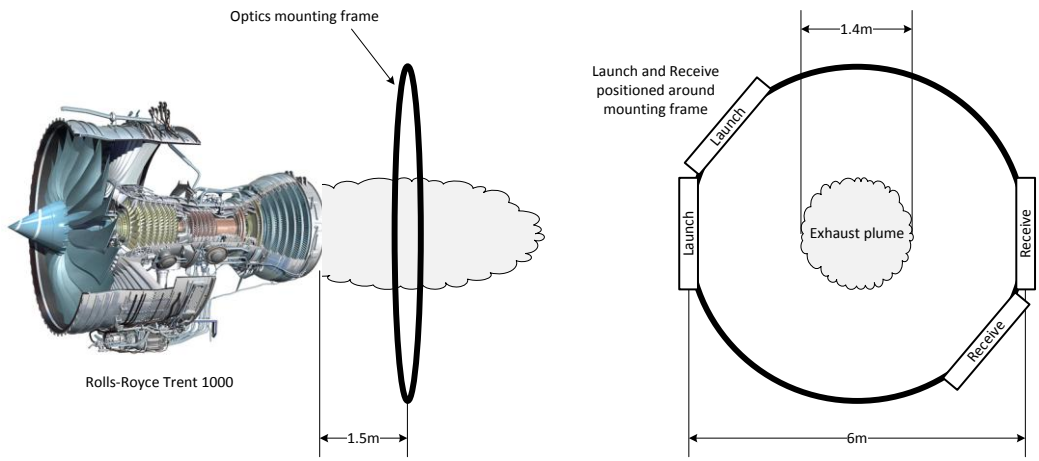

Fig. 2. Geometric arrangement of beam array with respect to the engine and exhaust plume.

The beam array is located on a custom-built circular mounting frame 6m in diameter and positioned 1.5m aft of the engine exhaust outlet. The engine exhaust is a 1.4m diameter plume comprising an annulus of 18 burners. The optics mounting comprises several launch with a set of diametrically opposite receive optic-plates which provide both structural support for the mounting frame and a spread of angular projections around the imaging space.

The traditional approach to beam array design is to implement a geometrically determined parallel beam rectilinear (regular) array. There are 2 considerations for a geometrically determined regular array; 1) the number of projections, 2) the number of beams per projection. The number of projections is selected based on optic-access to the imaging space and the size of the imaging space with the projection width being the diameter of the imaging space. The number of beams per projection is determined by the physical constrains of the optics on both the launch and receive side, and the projection width. With the above information the design of a geometrically determined regular array can be automatically generated.

For the arrangement in Fig. 2, Fig. 3 shows geometrically determined regular arrays for 4 projections with 32 beams per projection (a), 5 projections with 25 beams per projection (b), and 6 projections with 21 beams per projection (c):

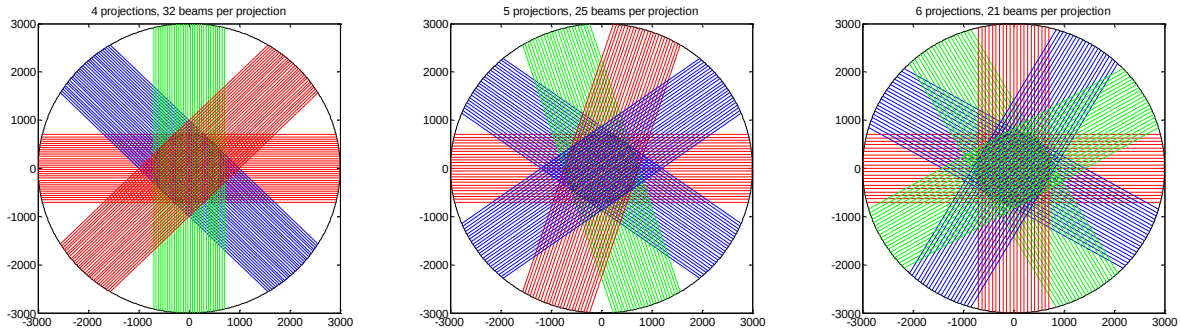

Fig. 3. Examples of geometrically determined arrays with between 120 and 130 beams: 4x32 (a), 5x25 (b), and 6x21.

The problem with geometrically determined regular arrays is that they only take account of the physical parameters of the problem and do not account for factors associated with the beam paths transecting the imaging space. Therefore a method for designing beam arrays is required that considers not only the physical constraints of the problem but also the beam paths in the imaging space and their impact on reconstruction performance.

3. Determining reconstruction accuracy

The Daun Group at Waterloo have presented a method for developing optimised beam array designs based on the properties of the resolution matrix [5]. This work builds on previous work on resolution matrices for geophysics tomography applications [12]. The resolution matrix is used to define a fitness value, which is a function of design parameters that specify the beam configuration.

3.1. Tikhonov regularisation

The limited-data nature of the problem means that there are regions of the imaging space where no measurement data exists. Consequently there is a large null space resulting in an underdetermined problem which is not directly invertible. Image reconstruction for laser absorption tomography using Tikhonov regularisation has been described in [13]. The regularised inverse can be expressed as:

$$\mathbf{A}^{\#} = \left(\mathbf{A}^{\mathrm{T}}\mathbf{A} + \lambda^2 \mathbf{L}^{\mathrm{T}}\mathbf{L}\right)^{-1}\mathbf{A}^{\mathrm{T}} \tag{2}$$

The **L** matrix is an approximation to the gradient function which adds the property of smoothness, or high-frequency noise filtering, to the image reconstruction by spanning the null space. The relaxation parameter controls the influence of this smoothness on the reconstructed images.

3.2. Resolution matrices and fitness value

Using the regularised inverse, the reconstructed solution can then be determined by:

$$\mathbf{x}_{\lambda} = \mathbf{A}^{\#}\mathbf{b} = \mathbf{A}^{\#}\mathbf{A}\mathbf{x}^{\mathbf{exact}} + \mathbf{A}^{\#}\boldsymbol{\delta}\mathbf{b} = \mathbf{R}\mathbf{x}^{\mathbf{exact}} + \mathbf{A}^{\#}\boldsymbol{\delta}\mathbf{b} \tag{3}$$

Where the measurement vector can be expressed as the sum of the true measurement plus some noise component, i.e. $\mathbf{b} = \mathbf{b}^{\mathbf{exact}} + \boldsymbol{\delta}\mathbf{b} = \mathbf{A}\mathbf{x}^{\mathbf{exact}} + \boldsymbol{\delta}\mathbf{b}$. The resolution matrix, **R**, is defined as the product of the sensitivity matrix and the regularised inverse, whereas $\mathbf{A}^{\#}\,\boldsymbol{\delta}\mathbf{b}$ is the perturbation error associated with noise amplification in the reconstruction.

In an ideal experimental where $\boldsymbol{\delta}\mathbf{b} = \mathbf{0}$, the reconstructed solution equals the exact solution where $\mathbf{R} = \mathbf{I}$. This implies each pixel in the image can be independent determined from the measurement data and assumes that

each pixel is of equal importance to the reconstruction. A fitness value, which seeks to minimise the distance between **R** and **I** and thus converge the reconstructed solution to the exact solution, can be expressed as:

$$F = \left\| \mathbf{R} - \mathbf{I} \right\|_F^2 \tag{4}$$

A notable feature of the fitness value is that since the resolution matrix is only dependent on the sensitivity matrix, which is a function of the beam layout, then optimisation based on reduction of the fitness value results in optimised beams arrays that are independent of the CO_2 concentration profile in the exhaust plume.

The reconstruction error can be expressed as the absolute mean percentage error between the exact and reconstructed solutions:

$$err = \frac{\left\| \mathbf{x}^{\mathbf{exact}} - \mathbf{x}_{\lambda} \right\|}{\left\| \mathbf{x}^{\mathbf{exact}} \right\|} \tag{5}$$

4. Optimising beam array designs using resolution matrices

Using the resolution matrix and fitness value, the beam array optimisation is supplemented with design parameters which impose real constraints on the optimisation. Each constraint constitutes an optimisation variable.

4.1. Optimisation constraints

Design constraints are chosen to emphasise properties of the imaging problem and impose real physical limits on the practicality of implementing a given array design for a real laser absorption tomography system. All optimisations will only consider the beam arrangement in the plume space as this is the region where determination of the CO_2 distribution is required. For real limited-data beam arrays for in-plume imaging in gas turbine engines there are 3 constraints considered:

1. **Array type**; either *regular* arrays which have fixed diametric launch and receive pairings, or *irregular* arrays which have variable launch and receive pairings.
2. **Problem symmetry**; encompassing both *projection-symmetry* where symmetry exists at a projection level, and *radial-symmetry* which forces the property of projection-symmetry radially around the beam array.
3. **Variable optic position**; which considers the positional variation of both the launch and receive optics within a projection around the imaging space. This design constraint imposes a limit on the closeness to which optics can be located because of the physical size of the launch and receive optics.

4.2. Beam array optimisation method

Optimisation of the beam arrays will use a Genetic Algorithm (GA) to traverse the large search space of constrained beam arrays. Fig. 4 illustrates the basic algorithm for beam array optimisations incorporating the GA:

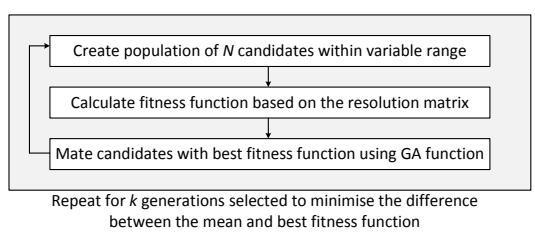

Fig. 4. Algorithm for beam array optimisation.

On the first iteration, a population of 1000 random seed arrays is generated based on the physical constraints imposed in section 4.1 for which the fitness value is calculated using Equation (4). For the 20 arrays with the best (lowest) fitness value, a new population of 1000 arrays is created by the GA with the same physical constraints. This sequence constitutes a "generation". The process of fitness value calculation and optimal array creation continues until either the mean and best fitness for a 1000 array population has converged, or 10 generations has completed. The optimisation simulations are developed using Matlab with the Global Optimization Toolbox [14].

4.3. Optimisation test cases

Table 1 summarises the beam array optimisation test cases which will be simulated outlining the array type, constraints, and number of simulation variables:

Table 1. Beam array optimisation test cases.

Test case	Array type	Optimisation constraints	Variables
1	Regular	Fixed L/R position, single spacing for all projections	1
2	Regular	Fixed L/R position, single spacing per projections	6
3	Irregular	Fixed L/R position, variable L/R pairings	126
4	Irregular	Fixed L/R position, variable L/R pairings, projection and radial symmetry	10
5	Irregular	Variable L/R position, variable L/R pairings, projection and radial symmetry	20

5. Results and discussion

For each of the test cases the optimised beam array is determined based on minimisation of the fitness value. Images are reconstructed using Tikhonov regularisation and the associated reconstruction error relative to a quasi-realistic phantom is calculated.

5.1. Beam array optimisation results

The fitness optimisation results per generation of the GA and the optimised beam arrays for each of the test cases in Table 1 are shown in Fig. 5:

	Fitness Optimisation Result	Optimised Beam Array
Test case 1	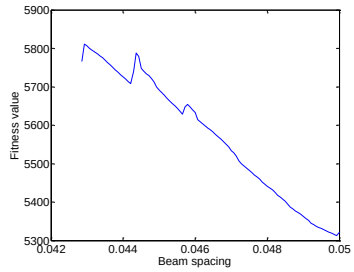	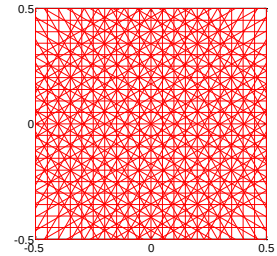
Test case 2	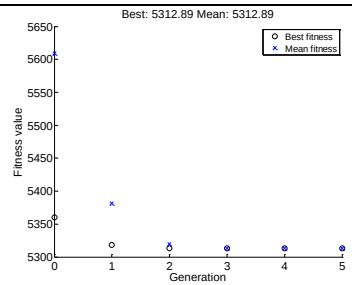	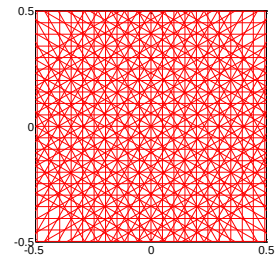
Test case 3	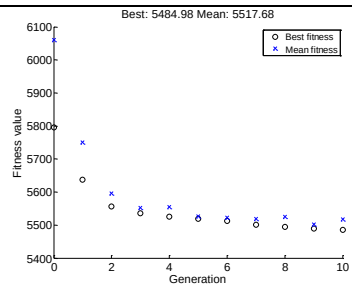	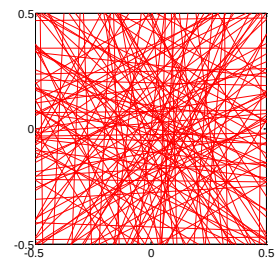
Test case 4	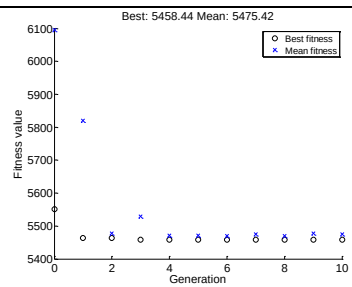	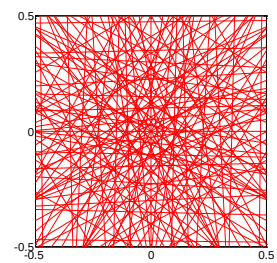
Test case 5	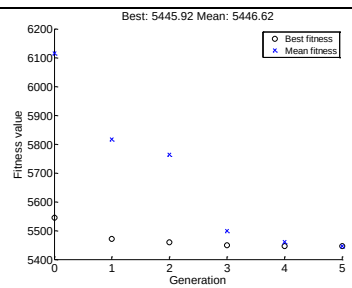	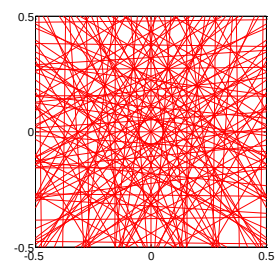

Fig. 5. Fitness optimisation result and optimised beam array for each test case simulation.

5.2. Reconstruction results

For each of the optimised beam arrays, the reconstruction of a quasi-realistic exhaust plume phantom with an annulus of 18 burners on a 70x70 mesh without measurement noise, and the calculated reconstruction error is shown in Fig. 6:

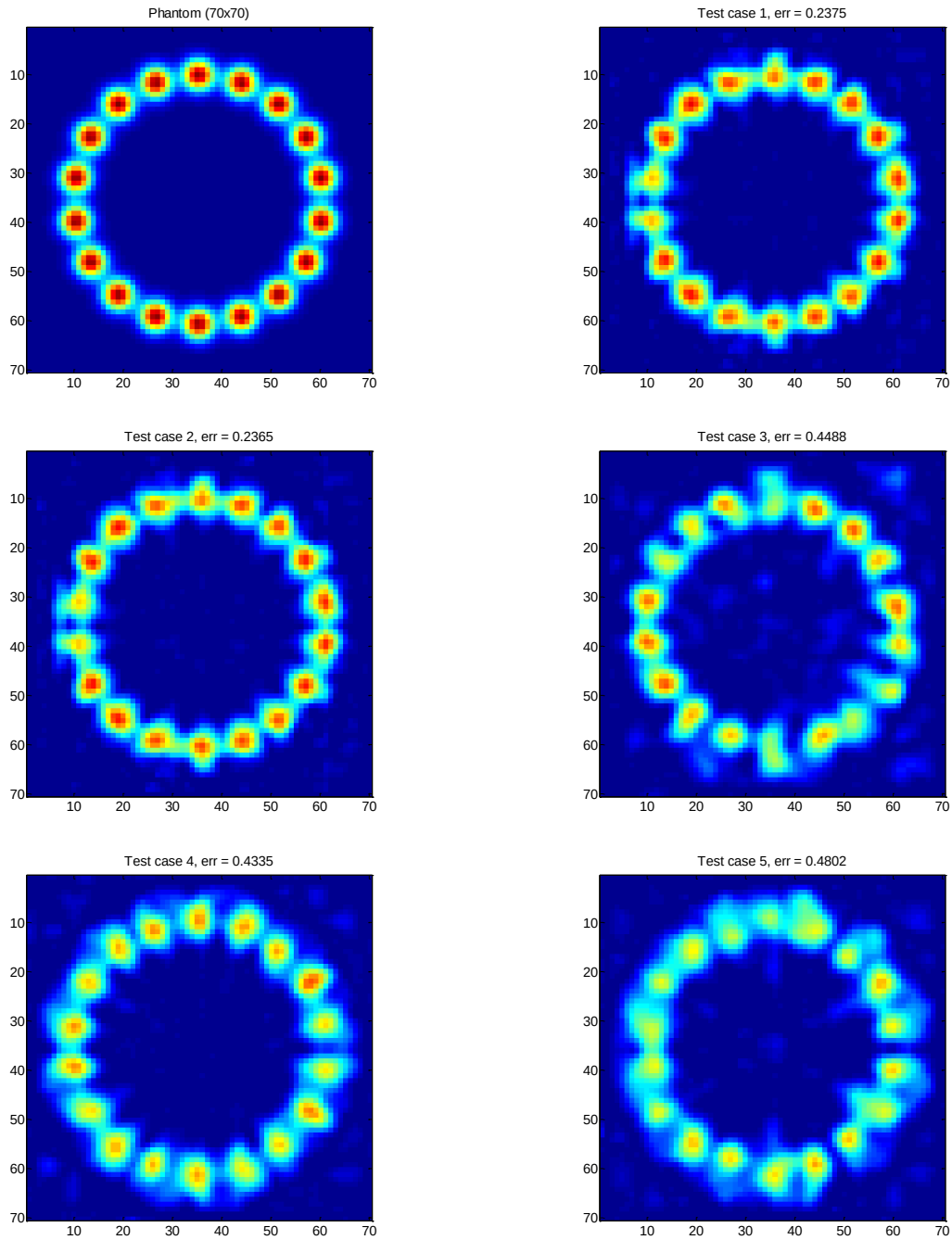

Fig. 6. Reconstructed images for 18 burner quasi-realistic phantom for each test case optimised beam array.

Fig. 7 shows the relationship between the fitness value and corresponding reconstruction error for each optimised beam array test case:

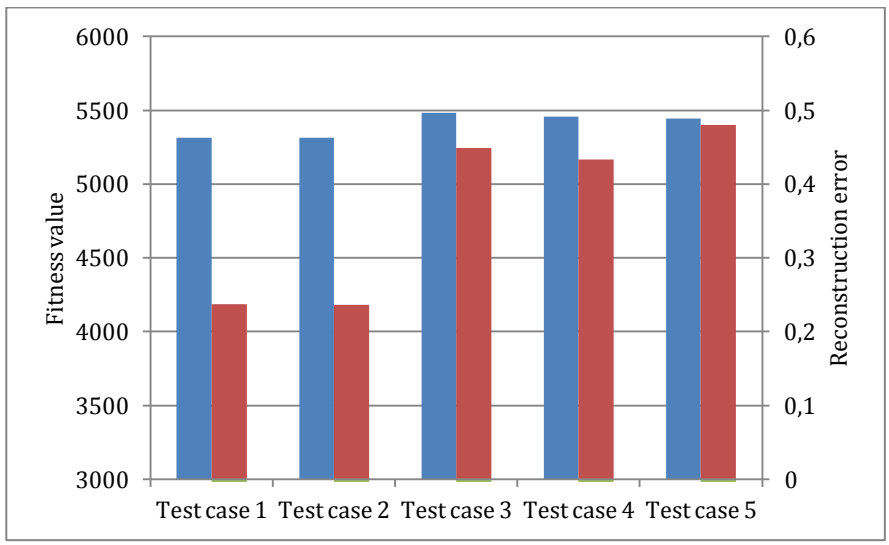

Fig. 7. Fitness values and reconstruction errors for each optimised beam array test case.

5.3. Discussion and analysis of beam array optimisation and reconstruction results

The optimisation results strongly suggest the regular array is a preferential design decision compared to an irregular array. Overall there is an improvement of the calculated fitness value of around 2% which translates into a halving of the reconstruction error – this is highly evident in the visual quality of the reconstructed images of the quasi-realistic exhaust plume phantom. In this design, regular arrays have a good angular spread because of the use of 6 projections spaced at 30° around the plume. Furthermore the beam density on the projections is high, with 21 beams spaced at 50mm optics pitch, giving a good sampling of the imaging space.

The expectation is that an irregular array might be able to sample the imaging space more effectively however the imposed physical constraints limit the degrees of freedom the optimisations have. As an example, for a 1.4m projection and 6m beam pitch length the maximum angular variation is just 13°; when coupled with either fixed or constrained variable launch and receive optic positions the range of variation in the beam paths is limited.

Although constraints do limit the search space by reducing the number of optimisation variables, it is still very large, and the optimisation simulations are only sampling a small subset of the possible beam arrangements. It is conceivable that given enough time to traverse the search space irregular array optimisations could converge to an optimal regular array; the formation of the partially regular beam structure at the centre of the test case 5 optimised array appears to support this possibility.

From the results some general observations are that for regular arrays the widest beam spread in all projections gives the optimal arrangement. This is an intuitive result as it implies better imaging performance results from a wider sampling of the imaging space. For irregular arrays, the property of symmetry appears to improve the arrangement with a 0.4% improvement in fitness giving a 3% reduction in the reconstruction error. Variable launch and receive positions gives a marginal improvement in fitness however, counter intuitively, the reconstruction error is notably higher; this is highly evident in the reconstructed images.

In the reconstructed images for both regular and irregular arrays, there is a notable difference in the structure and shape of the individual burners; this is possibly because of the coarseness of the 70x70 grid used for the reconstruction. A closer inspection of the ideal phantom shows that at the pixel level the actual values of the Gaussian phantoms are subtly different. The implication of this is that the coarseness of the grid is introducing discretisation noise into the reconstructed images. This could be in part overcome by the use of a finer mesh; however this would increase the underdetermined nature of the problem.

In addition to discretisation noise from the reconstruction grid, other limitations in the present study include the lack of measurement noise added to the data for the reconstructions precluding the determination of the spatial resolution for a given burner feature, and the idealised nature of the phantom used which, as a set of Gaussian phantoms, is not sufficiently realistic for a true representation of a gas turbine exhaust plume flow regime.

6. Conclusions

A structured approach to the design of a 126 beam, 6m absorption tomography array has been detailed. The concepts of the resolution matrix and fitness value have been outlined and real physical design constraints have been considered. Results from optimisation simulations to determine the optimal beam array based on minimising the fitness value have been presented along with reconstructed images with indications of the reconstruction errors. Overall the results demonstrate the feasibility of using resolution matrices with design constraints to design optimised beam arrays which can be readily implemented in a laser absorption tomography system for imaging concentrations of CO_2 in the exhaust plume of a Rolls-Royce Trent 1000 gas turbine engine.

Acknowledgements

The authors would like to express their thanks to Michael Croucher at the University of Manchester for his assistance with the optimisation simulations.

References

[1] Ibrahim, S., Green, R.G., Dutton, K., Evans, K., Abdul Rahim, R., Goude, A., 1999. Optical sensor configurations for process tomography, Measurement Science and Technology 10, pp. 1079-1086.

[2] Pal, S., Ozanyan, K.B., McCann, H., 2008. A computational study of tomographic measurement of carbon monoxide at minor concentrations, Measurement Science and Technology 19, 094018.

[3] Wright, P., Terzija, N., Davidson, J.L., Garcia-Castillo, S., Carcia-Stewart, C.A., Pegrum, S., Colbourne, S.M., Turner, P.J., Crossley, S.D., Litt, T.L., Murray, S.C., Ozanyan, K.B., McCann, H., 2010. High-speed chemical species tomography in a multi-cylinder automotive engine, Chemical Engineering Journal 158, pp. 2-10.

[4] Terzija, N., Davidson, J.L., Garcia-Stewart, C.A., Wright, P., Ozanyan, K.B., Pegrum, S., Litt, T.J., McCann, H., 2008. Image optimization for chemical species tomography with an irregular and sparse beam array, Measurement Science and Technology 19, 094007.

[5] Twynstra, M.G., Daun, K.J., 2012. Laser-absorption tomography beam arrangement optimization using resolution matrices, Applied Optics 51, pp. 7059-7068.

[6] FLITES : Fibre-Laser Imaging of gas Turbine Exhaust Species, 2012. EPSRC Ref. EP/J002151/1.

[7] Verhoeven, D., 1993. Limited-data computed tomography algorithms for the physical sciences, Applied Optics 32, pp. 3736-3754.

[8] Wright, P., Garcia-Stewart, C.A., Carey, J.S., Hindle, F.P., Pegrum, S.H., Colbourne, S.M., Turner, P.J., Hurr, W.J., Litt, T.L., Murray, S.C., Crossley, S.D., Ozanyan, K.B., McCann, H., 2005. Towards in-cylinder absorption tomography in a production engine, Applied Optics 44, pp. 6578-6592.

[9] Ma, L., Li, X., Sanders, S.T., Caswell, A.W., Roy, S., Plemmons, D.H., Gord, J.R., 2013. 50-kHz-rate 2D imaging of temperature and H2O concentration at the exhaust plane of a J85 engine using hyperspectral tomography, Optics Express 21, pp. 1152-1162.

[10] Fried, A., Richter, D., 2006. Infrared absorption Spectroscopy, in Analytical Techniques for Atmospheric Measurements, Blackwell Publishing.

[11] Constantino, E.P.A., Davidson, J.L., Ozanyan, K.B., 2007. "Comparison of two methods for tomographic imaging from severely incomplete data," 5th World Congress on Industrial Process Tomography, Bergen, Norway.

[12] Menke, W., 1989. Geophysical Data Analysis: Discrete Inverse Theory, Academic Press, pp. 51-65.

[13] Daun, K.J., 2011. Infrared species limited data tomography through Tikhonov regularisation, Journal of Quantitative Spectroscopy and Radiative Transfer 111, pp. 105-115.

[14] The Mathworks Inc., 2013. Global Optimization Toolbox, available at http://www.mathworks.co.uk/products/global-optimization/.